Engineering Science and Technology, an International Journal 24 (2021) 533–542

HOSTED BY

Contents lists available at ScienceDirect

Engineering Science and Technology, an International Journal

journal homepage: www.elsevier.com/locate/jestch

Full Length Article

The influence of chromium content on wear and corrosion behavior of surface alloyed steel with $Fe_{(16-x)}Cr_x(B,C)_4$ electrode

Engin Kocaman [a,*], Bülent Kılınç [b], Mustafa Durmaz [c], Şaduman Şen [c], Uğur Şen [c]

[a] Zonguldak Bulent Ecevit University, Faculty of Engineering, Department of Metallurgical and Materials Engineering, Zonguldak 67100, Turkey
[b] Sakarya University of Applied Sciences, Vocational School of Arifiye, Machine and Metal Program, Sakarya 54800, Turkey
[c] Sakarya University, Faculty of Engineering, Department of Metallurgical and Materials Engineering, Sakarya 54100, Turkey

ARTICLE INFO

Article history:
Received 4 May 2020
Revised 1 August 2020
Accepted 6 August 2020
Available online 29 August 2020

Keywords:
Hardfacing
Surface alloying
Hardness
Wear
Corrosion

ABSTRACT

In this study, the electrodes containing $Fe_{(16-X)}Cr_X(B,C)_4$ (X = 3,4,5) were used for surface alloying on an AISI 1010 steel substrate. The alloy structure of the coating exhibits in-situ composite structure with a large amount of reinforcing carbides and borides phases as to be hypoeutectic and hypereutectic structure in the surface alloyed layer. The obtained composition of the alloy shows that it contains much more interstitial hard phases in the alloyed layer than the conventional hardfacing alloys used in the industrial applications for the hardfacing of the steels. The morphological and microstructural properties showed that layer microstructure changed from hypoeutectic to hypereutectic structure with an increase in chromium content. The results of these studies revealed that the microstructure of hardfacing layers consists of interstitial phases of α(Fe-Cr) and $(Fe,Cr)_{23}(C,B)_6$ as major phases, $(Fe,Cr)_2(C,B)$ and $(Fe,Cr)_7(C,B)_3$ as minor phases in the in-situ composite structure. The composite hardness' in the alloyed surface layers of the $Fe_{(16-X)}Cr_X(B,C)_4$ alloys ranged from 711 HV to 1164.3 HV. Wear test against alumina ball shows that the friction coefficients of the surface alloyed layers decreased with increase in applied loads and decrease in chromium content in the $Fe_{(16-X)}Cr_X(B,C)_4$ alloy composition. Coefficient of friction ranged from 0.55 to 0.79 in the present study. Wear rates of the surface alloyed steels caused to increase with decrease in chromium content and increase in applied loads. The wear rates of the alloyed layer changed between 3.07 × 10 and 5 mm3/m and 6.95 × 10^{-5} mm^3/m. The corrosion resistance of the alloyed layers was measured by a potentiostatic polarization test. I_{corr} and E_{corr} of the coated layers changed from 1.813 to 9.965 μA/cm^2 and −704.786 to −745.792 mV, depending on alloyed layer compositions. With increasing chromium content, the corrosion resistance of the coating layer has changed in a nobler side.

1. Introduction

The need for machine parts used in aggressive working conditions is increasing day by day in the modern world. Parts working under these conditions are exposed to surface losses with wear and corrosion. Since the replacement of these parts will cause high operating costs, service times can be extended with a suitable coating process on the part surface. Today, many methods, such as thermal spray, cladding, and welding, are used in the surface coating processes of machine parts. Various surface alloys can be coated on to an appropriate substrate using thermal spraying, cladding, and welding techniques [1,2]. However, welding is key technology due to its economically and higher deposition rate compared with the others. Many welding methods such as shielded manual arc welding (SMAW) [3], submerged arc welding (SAW) [4], gas tungsten arc welding (GTAW) [5], plasma transferred arc welding (PTA) [6], flux cored arc welding (FCAW) [7]. Laser metal deposition (LMD) [8] processes are mostly used for surface alloying treatment. However, among all these methods SMAW is come forward from the others because of its higher mobility and deposition rate along with economical benefits. Also, an increasing number of hardfacing alloys can be applied using the SMAW method in the industry.

In many industrial applications, iron-chromium-carbon based electrodes are used to increase the surface hardness, wear, and corrosion resistance of the steels. On the surfaces covered with electrodes with this composition, structures such as hypoeutectic, eutectic, and hypereutectic are obtained according to the electrode composition [9,10]. The properties of coating vary depending on factors such as the amount, distribution, and morphology of the

* Corresponding author at: Zonguldak Bulent Ecevit University, Faculty of Engineering, Department of Metallurgical and Materials Engineering, Zonguldak 67100, Turkey (E. Kocaman).
E-mail address: enginkocaman@beun.edu.tr (E. Kocaman).
Peer review under responsibility of Karabuk University.

https://doi.org/10.1016/j.jestch.2020.08.003
2215-0986/

hard carbides of the transition metals such as MC, M_2C, M_3C, M_7C_3, and $M_{23}C_6$ formed in-situ in the structure [11–13]. It is also known that chromium is a strong boride forming element. Additionally, a small amount of boron in the Fe-Cr system causes the stabile borides of transition metals such as MB, M_2B, M_5B_3, MB_4 can form [14–16]. In the case of carbon and boron in the hard surface alloy composition at the same time, the alloy structure shows the in-situ composite structure, including the ductile α-phase and the hard phases of carbides and borides of transition metals. The microstructure can exhibit hypoeutectic (α-eutectic(α + M_x(C,B)), eutectic (α-M_x(C,B)) and hypereutectic (eutectic(α + M_x(C, B) + M_x(C,B) blocky phase) microstructures. The alloyed layer, including these microstructures, plays a crucial role in the wear and corrosion resistance of the alloyed layers [17,18].

Both manufacturers and researchers have been developing specialized welding electrodes for industrial applications. Fe-Cr-C alloys are very popular with the use of other welding methods. However, there are limited researches on $Fe_{(16-X)}Cr_X(B, C)_4$(X = 3,4,5) coatings produced by shielded manual arc welding (SMAW). In this paper, Fe-Cr-B-C based hardfacing electrodes containing various amounts of chromium and boron along with carbon were developed by SMAW, and their microstructural observation and corrosion behaviors were investigated.

2. Experimental

Three types of electrodes were prepared and used as hardfacing alloys in the SMAW process. The electrodes were coated with different compositions of the powder mixtures of ferrous chromium containing high carbon (Fe–Cr (HC)), ferrous boron (Fe–B), and Armco iron powders together with fluxes. Rutile (TiO_2), calcium carbonate ($CaCO_3$), calcium fluoride (CaF_2), silica (SiO_2), alumina (Al_2O_3), and some additives like K-alginate and potassium silicate ($K_2O.SiO_2$) binder were used as flux materials together with ferrous alloys. Composition of the hardfacing electrodes cover $Fe_{(16-X)}Cr_X(B,C)_4$ (X = 3,4,5), see Table 1. The core wire of the electrode was H08A stick with a diameter of 2.5 mm. The diameter of the coated electrode is about 5.5 mm. The compositions of H08A, Fe–Cr(HC), and Fe–B alloys are given in Table 2.

The hardfacing was carried out on AISI 1010 plain carbon steel substrate (see Table 3) by means of the SMAW process with direct current reverse polarity. The dimensions of the substrate used for the surface alloying treatment were 70 mm in length, 30 mm in width, and 8 mm in thickness. The deposition was carried out in the flat position; the current and travel speed was fixed in all tests. In order to reduce the effect of dilution, the hardfacing bead was deposited as two layers; the total thickness of the hardfacing layer was about 4–6 mm. The welding parameters were as follows: the welding current is 120–130 A, arc voltage is 20–25 V, and the travel speed is 25–30 cm/min.

Microstructures were observed with scanning electron microscopy (SEM) (JEOL-JSM-6060). The phase analysis of the hardfacing layer formed on the steel substrate was determined by X-ray diffraction analysis with Cu-K_α radiation; the compositions of the formed phases in the alloyed layers were investigated using electron dispersive spectroscopy (EDS). The hardness of the seam section was measured with Vickers-Hardness (Future-Tech FM 700) at 0.5 mm intervals from the substrate material to the top of coating. All the samples were cut from cross-section and grinded with emery papers up to 1200 grid and polished with 0.3 μm Alumina paste. Ultrasonically cleaned samples with ethyl alcohol was etched with 3%Nital solution before the microstructural examinations.

Ball-on-disk reciprocal wear test was carried out in dry sliding conditions at room temperature using a friction and wear tester (TRİBOtechnic-TRIBOtester). The ball material of the wear couple was Al_2O_3 (1850 $HV_{0.1}$). The diameter of the alumina ball was 10 mm. The tested specimens were machined to block with the size of 50 mm × 30 mm × 10 mm. The wear conditions were a normal loads of 2 N, 5 N and 8 N with a sliding speed of 30 mm.s^{-1} and a sliding distance of 200 m.

The wear volume was calculated using Eq. (1)

$$V = A.l \tag{1}$$

where l is the track line formed on the worn surface (mm) and A is the crosscut track area of the worn path (mm^2) measured with 3D optical (Huvitz) profilometer. The wear volume loss was calculated after a certain time interval. The coefficient of friction (COF) was calculated with the formulas of Eq. (2);

$$COF = \frac{F_s}{F_N} \tag{2}$$

where COF represents the friction coefficient, Fs is the lateral force (N) recorded during the sliding time and F_N is the applied normal load (N). A real time by a computerized data acquisition system was used recorded the friction coefficient of the hardfacing layer. Wear rate (WR) of the hardfacing layer via alumina ball was calculated using the formula;

$$WR = V/S \tag{3}$$

where V is the wear volume and S is the sliding distance (m). Corrosion test was carried out using the potentiodynamic polarization method according to ASTM G59-97. All electrochemical

Table 1
Atomic percentages of chromium, boron in the prepared electrodes cover (%at.)

Compound	Cr	% B	% C	Fe
$Fe_{13}Cr_3(B,C)_4$	15	10	10	Bal.
$Fe_{12}Cr_4(B,C)_4$	20	10	10	Bal.
$Fe_{11}Cr_5(B,C)_4$	25	10	10	Bal.

Table 2
Composition of the powders used in electrode coer (%at.)

	C	Cr	B	Mn	Si	Fe
H08A	<0.1	0.064	–	0.35–0.40	0.10	Bal.
Ferro-Cr	6.81	68.21	–		0.51	24.468
Ferro -B	0.312	–	18.58		0.39	80.602

Table 3
The chemical composition of AISI 1010 Steel substrate.

C	Si	Cr	S	P	Mn	Fe
0.09	0.001	0.064	0.022	0.026	0.4	Bal.

measurements were performed using Gamry 300 electrochemical analyzer system (Warminster, PA, USA) equipped with a paraCell electrochemical cell for corrosion with a waterproof gasket, leaving an exposed area of 1 cm^2 on the hardfaced surface for corrosion and the data were analyzed in the Gamry EChem Analyst software package (Gamry Instruments, PA, USA). The potentiodynamic polarization tests were carried out at a scanning rate of 1 mV/s in a 3.5 wt% NaCl solution from −500 to +1.500 mV via standard calomel reference electrode (SCE) and graphite as the counter electrode. The tests were carried out at atmospheric conditions (25 °C) and humidity level of 31% (+/−1). To optimizing the results each corrosion tests were repeated three times using the constant conditions such as solution weight, solution temperature and the solution pH = 6. Polarization curves were obtained and I_{corr} (corrosion current), E_{corr} (corrosion potential), and R_p (polarization resistance) values were determined. Tafel plots were obtained by the intersection of cathodic and anodic corrosion current (Icorr) and corrosion potential (Ecorr) values. Accordingly, the following relation was used to determination of the corrosion rate:

$$CR = \frac{IcorKEW}{dA} \tag{4}$$

In the Eq. (4), K is a constant, EW is the equivalent weight in grams/equivalent, d is density in grams/cm^3, A is sample area in cm^2. Subsequently, the corrosion current was calculated according to the following relation:

$$icor = \frac{\beta a \beta c}{2.3Rp(\beta a + \beta c)} \tag{5}$$

where: βa and βc are the anodic and cathodic Tafel Constant, respectively on volts/decade.

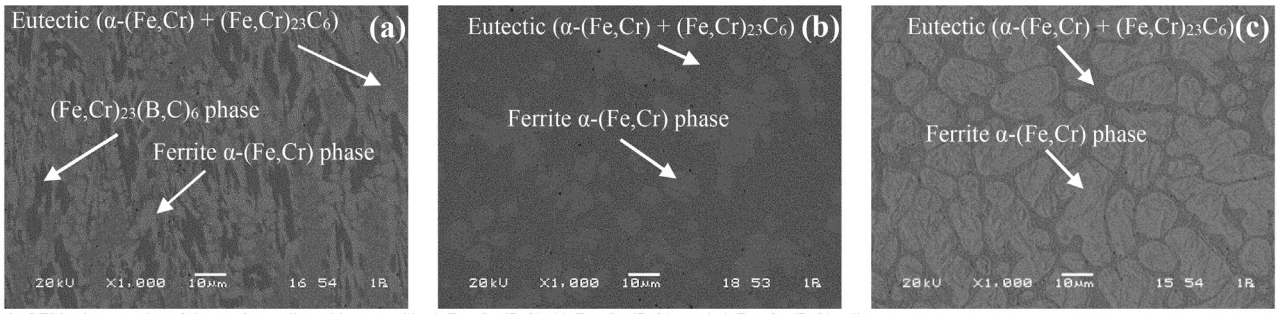

Fig. 1. SEM micrographs of the surface alloyed layers with a) $Fe_{11}Cr_5(B,C)_4$b) $Fe_{13}Cr_4(B,C)_4$ and c) $Fe_{12}Cr_3(B,C)_4$ alloys.

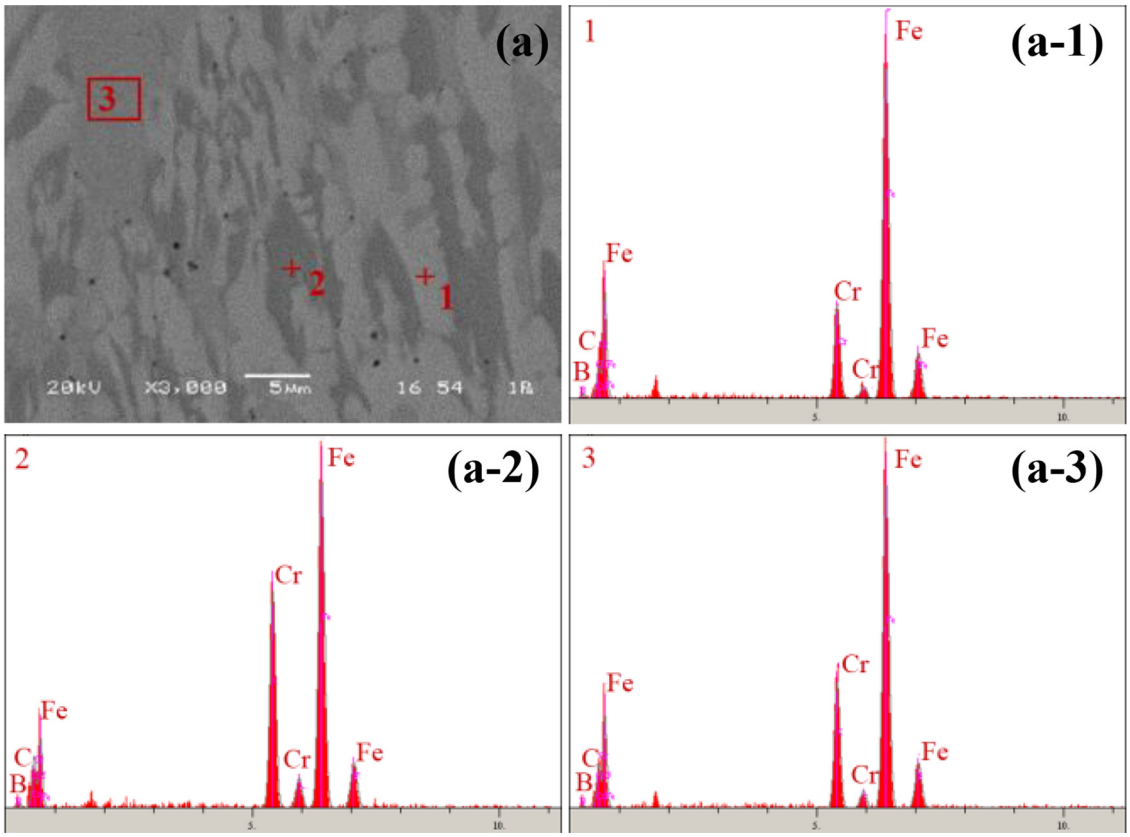

Fig. 2. SEM micrographs and EDS analysis of the surface alloyed steel samples a) $Fe_{11}Cr_5(B,C)_4$.

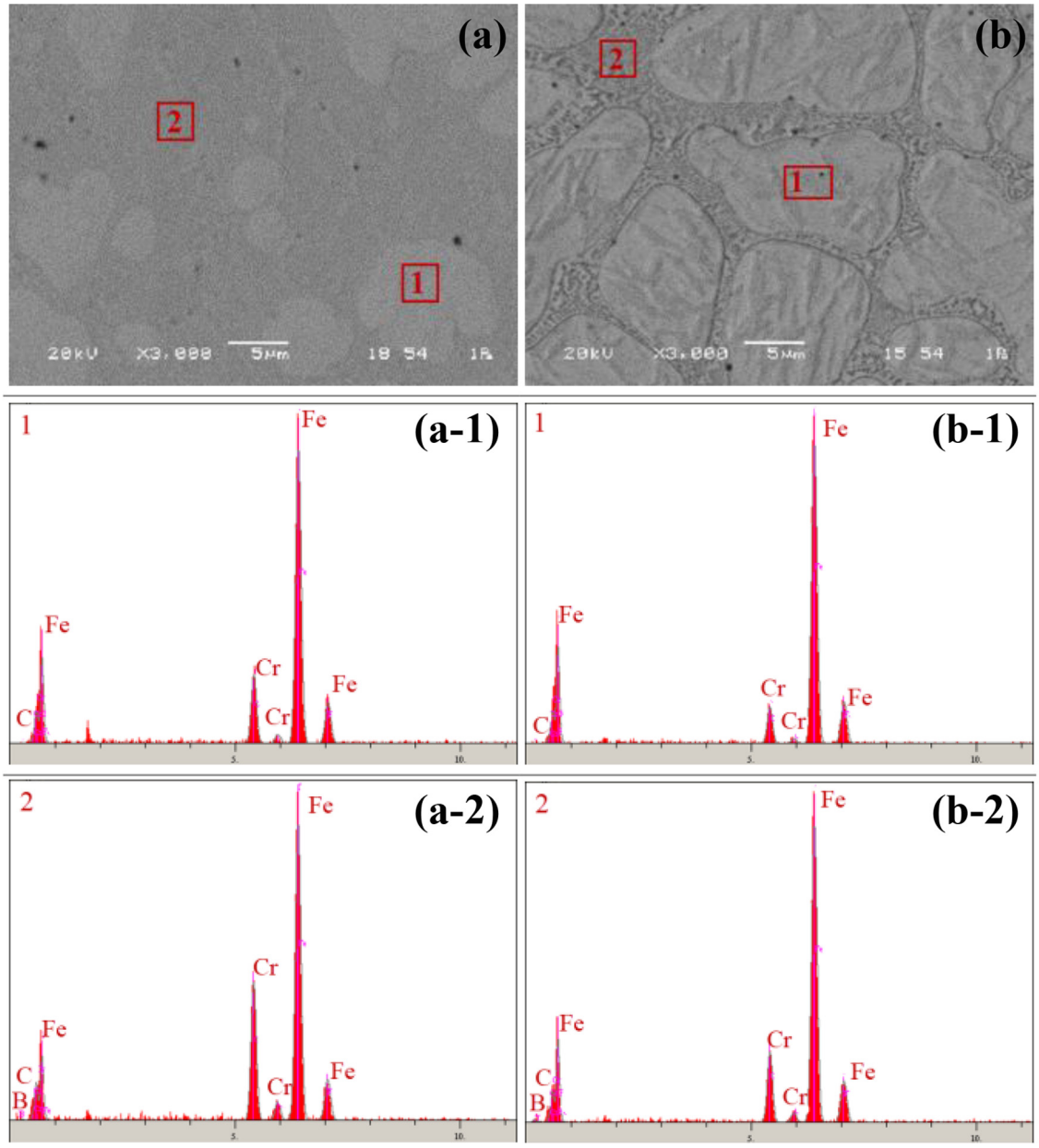

Fig. 3. SEM micrographs and EDS analysis of the surface alloyed steel samples a) $Fe_{12}Cr_4(B,C)_4$ and b) $Fe_{13}Cr_3(B,C)_4$ alloys.

3. Results

3.1. Microstructure and phases

Hardfacing electrodes including the different atomic percentages of chromium, boron, and carbon and fluxes coated on the steel substrate by SMAW process, and then quenched in air. The average coating layer thickness ranged from 4 to 5 mm and has a smooth surface and porosity free topography. SEM images of the coating layers are illustrated in Fig. 1. As shown in Fig. 1(a), the electrode of $Fe_{11}Cr_5(B,C)_4$ alloy caused the formation of hypereutectic microstructure. It was shown that the surface alloyed layer has a well distributed composite structure, including the eutectic matrix and primary blocky carbo-boride phase with dark color. Blocky carbo-borides formed in the coated layers have a sharp corner structure and were well-distributed in the matrix. Dark color boride phases were surrounded by a white color α-(Fe-Cr) phase. Fig. 1(b) and (c) show the microstructures of $Fe_{13}Cr_3(B,C)_4$ and $Fe_{12}Cr_4(B,C)_4$ compositions, which have a relatively low Cr ratio compared to the composition of the $Fe_{11}Cr_5(B,C)_4$ alloy. According to the microstructures, the presence of pre-eutectic primary ferrite (α-(Fe-Cr)) phase + eutectic (α-(Fe-Cr) + $M_{23}C_6$) structures were revealed. Also, the eutectic regions decreased with the decrease of Cr ratio, as shown in the microstructures. The white regions took place in the microstructure considered as a primary ferrite, that increased with the decrease of chromium.

Figs. 2 and 3 show the cross-sectional SEM images and EDS analysis of the surface alloyed layers with the composition of $Fe_{11}Cr_5(B,C)_4$, $Fe_{12}Cr_4(B,C)_4$ and $Fe_{13}Cr_3(B,C)_4$. It is seen that Fe and Cr peaks are present in the region indicated as primary ferrite, and Fe and B peaks, as well as B and Cr peaks, are found in the EDS

analysis taken from eutectic structure. It can be understood from here that it supported the idea of the white block phases are primary ferrite, and the eutectic structure consists of (α-(Fe-Cr) + $M_{23}(C,B)_6$) phases.

XRD analysis of the surface alloyed layer showed that the major phases formed in are α-(Fe-Cr) and $M_{23}(C,B)_6$ phases (M = Fe,Cr), see Fig. 4. XRD analysis shows that, all compositions of the surface alloyed layers has similar phases. However, SEM images, EDS analysis, and elemental maps showed that the $Fe_{11}Cr_5(B,C)_4$ composition presents the hypereutectic microstructure which has blocky hard carbo-boride primary phase of ($(Fe,Cr)_{23}(C,B)_6$) together with eutectic (α-(Fe-Cr)+$(Fe,Cr)_{23}(C,B)_6$) along with minor $(Fe,Cr)_2(C,B)$ and $(Cr,Fe)_7(C,B)_3$ phases. J.X. Gong et al. explained that the microstructure of the Fe-Cr-B-C hardfacing alloys consists of ferrite, austenite, martensite and borides of $(Fe, Cr)_2B$, $(Fe, Cr)_{23}(C, B)_6$, (Fe,Cr)B and $(Fe,Cr)_3(B,C)$ [19]. In the present study, α-(Fe-Cr) solute solution and major $(Fe,Cr)_{23}(C,B)_6$ carbo-boride phase exist together with minor $(Fe,Cr)_2(C,B)$ and $(Cr,Fe)_7(C,B)_3$ phases. (Fe, Cr)B and $(Fe,Cr)_3(B,C)$ phases were not detected for any alloy compositions.

Cr-C binary phase diagram shows that hypereutectic compositions initially lead to the formation of Cr_7C_3 minor phase under the liquidus line. Then Cr_7C_3 phase transforms into $Cr_{23}C_6$ phase with peritectic reactions. A peritectic is known as a reaction where a solid phase and a liquid phase will together form a second solid phase at the particular temperature and composition. In this case, $(Cr,Fe)_7(C,B)_3$ may remain untransformed in the system under rapid solidification conditions.

It is also known that Fe and B form a boride phase primarily in the Fe_2B structure. In the alloy systems, interstitial elements like C and B can take place with each other like substitution elements like Fe and Cr [20]. However, the pre-eutectic microstructure is observed in $Fe_{13}Cr_3(B,C)_4$ and $Fe_{12}Cr_4(B,C)_4$ compositions. Cr-C binary diagram shows that pre-eutectic compositions initially form α-phase under the liquidus. As the temperature decreased below the eutectic line, $Cr_{23}C_6$ phase took place in the microstructure in the α + eutectic form. As seen from Figs. 2 and 3 and Fig. 4, α-(Fe,Cr) + eutectic (α-(Fe-Cr)+$(Fe,Cr)_{23}(C,B)_6$) microstructure formed. However, decreasing the chromium and carbon content leads to increased α-(Fe-Cr) content and decreased the eutectic (α-(Fe-Cr) + $(Fe,Cr)_{23}(C,B)_6$) content in the microstructure. R. Shara et al. showed that $(Fe,Cr)_{23}(C,B)_6$ phase can be thermodynamically formed in all composition of Fe-Cr-C-B system with different C-B content [21]. Similarly, M.J. Duarte et al. explained that $(Fe,Cr)_{23}(C,B)_6$ major phases can be formed in the unstable metallic glass of the alloys, including Fe, Cr, Mo, B and C elements.

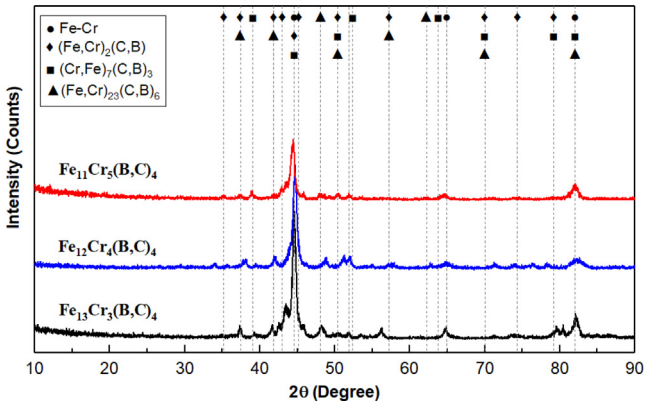

Fig. 4. XRD patterns of $Fe_{(16-X)}Cr_X(B,C)_4$ (X = 3,4,5) hardfacing coating.

3.2. Hardness and wear behavior

Hardness of the coated surface was measured at 0.3 mm intervals from the substrate to the end of the coating layer. The hardness of the hardfacing coatings is strongly dependent on the fraction of hard phases like carbides and borides in the microstructure [22,23]. The hardness values are given in Fig. 5 with line-scan. Therefore, the hard phase contents affect the composite hardness of the produced surface layer.

$Fe_{11}Cr_5(B,C)_4$ composition yields highest hardness, because it has much more carbo-boride phases than that of the $Fe_{13}Cr_3(B,C)_4$ and $Fe_{12}Cr_4(B,C)_4$ compositions. Whereas, $Fe_{13}Cr_3(B,C)_4$ has the fewest carbo-boride phase among all compositions. The composite hardness values of the surface alloyed layers increased with increase Cr, B, and C content, so it caused to form the higher carbo-boride phases in the alloyed layer. Hardness value increases with increasing Cr content in the compositions of $Fe_{13}Cr_3(B,C)_4$ to $Fe_{11}Cr_5(B,C)_4$, respectively. The hardnesses of the surface alloyed layers changed from between 711 and 1164.3 HV, depending on the alloy composition. Özel et all. obtained hardness values changing

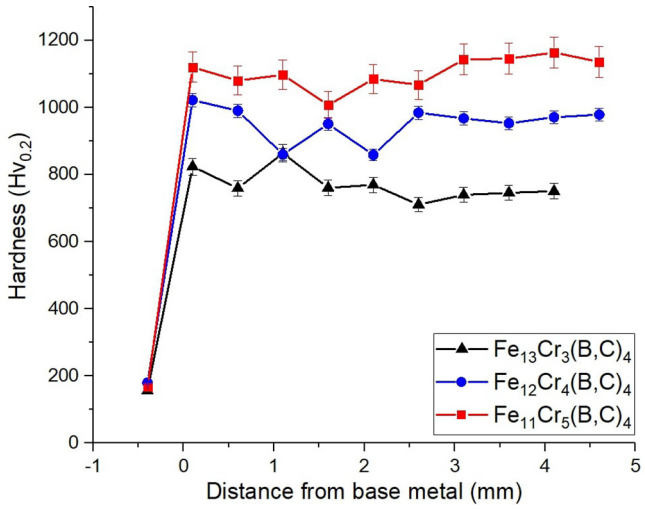

Fig. 5. Hardness distributions of the alloyed layers.

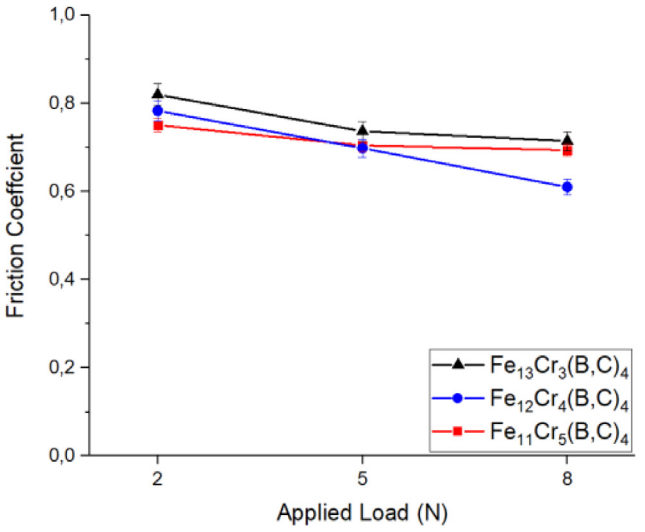

Fig. 6. Plots of friction soeffcient, depending on the sliding distance under 30 $mm.s^{-1}$ speed and 2 N-5 N and 8 N load.

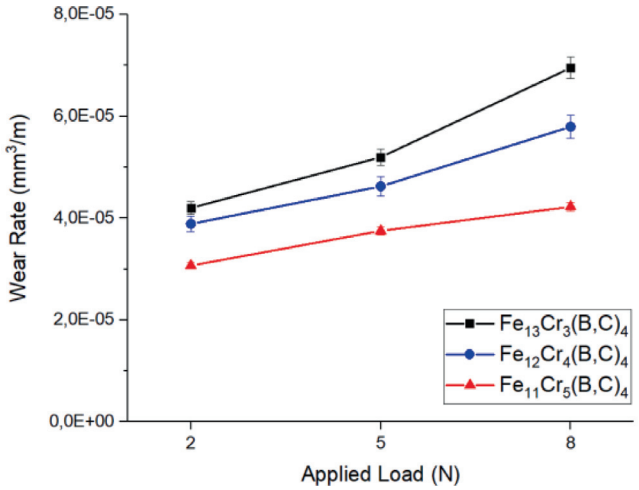

Fig. 7. Wear rate of coatings depending on the different loads.

between 580 Hv and 1200 Hv from the hardfacing study of Fe-Cr-B-C alloy carried out by PTA welding method. The results seem to be consistent with this study. However, methods that measure from a small point such as micro hardness in composite materials may not reflect the overall result. For this reason, it is important to measure macro hardness. In this study, macro hardness results were measured as 61.9 HRC (+/−0.5), 65.3 HRC (+/−0.4) and 68.3 HRC (+/−0.3), respectively, according to the increasing chromium ratio. In addition, the low standard deviation in the hardness results measured from the entire surface with 0.5 mm interval shows that the coating is performed homogeneously.

Fig. 6 shows the friction coefficient values obtained from the wear tests of the $Fe_{(16-X)}Cr_X(B, C)_4$ (X = 3,4,5) based electrodes coating layers on the steel surfaces against alumina (Al_2O_3) ball. It is seen in Fig. 6 that the coefficient of frictions of the alloys was changing between 0.55 and 0.79, depending on applied loads. C. Ozel et al. studied on the Fe-Cr-B-C surface alloyed steel, and they obtained friction coefficients between 0.5 and 0.75, which agrees with the present study [24]. G. Cui et al. studied on Fe-Cr-B alloys that the coefficient of friction against the SiC ball was about 0.45. İt is lower than that of the present study and Ozel et al. studies [24,25].

İt is possible that carbon addition leads to increases coefficient of friction along with SiC lubricant effects. As shown from the Fig. 6 that increase in load and decreasing Cr content in the alloys lead to the decreased coefficient of friction. It is possible that the increase in applied load caused the adhesion according to the softer α-phase increase in the microstructure and caused a little increase of friction coefficient of $Fe_{13}Cr_3(B,C)_4$ composition at highest load value (8 N). Fig. 7 shows that increase in applied load and decrease in Cr content in the alloyed layer caused to increase in wear rate. As shown from the results that the highest the hardness value, the highest the interstitial carbo-boride phases content and the highest the Cr, B, and C content caused to decrease the wear rates of the surface alloyed layers. Gibbs free energies of the chromium carbides and borides together with iron carbides and borides are much lower than that of the matrix. Also, covalent bonding of the interstitial atoms like boron and carbon make strong bonding force according to metallic bond of the iron and chromium atoms,

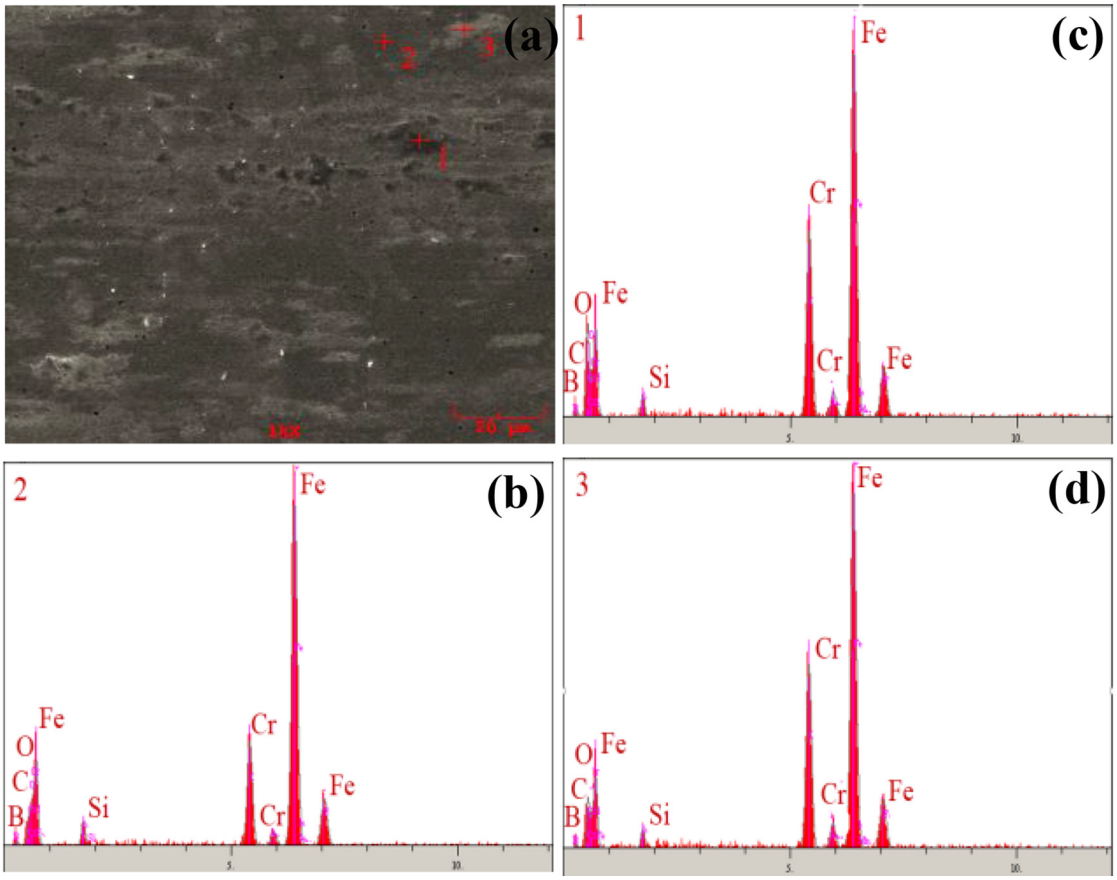

Fig. 8. Wear trace of $Fe_{12}Cr_4(B,C)_4$ composition under 5 N load (a) SEM microstructure (b)–(d) EDS analyses.

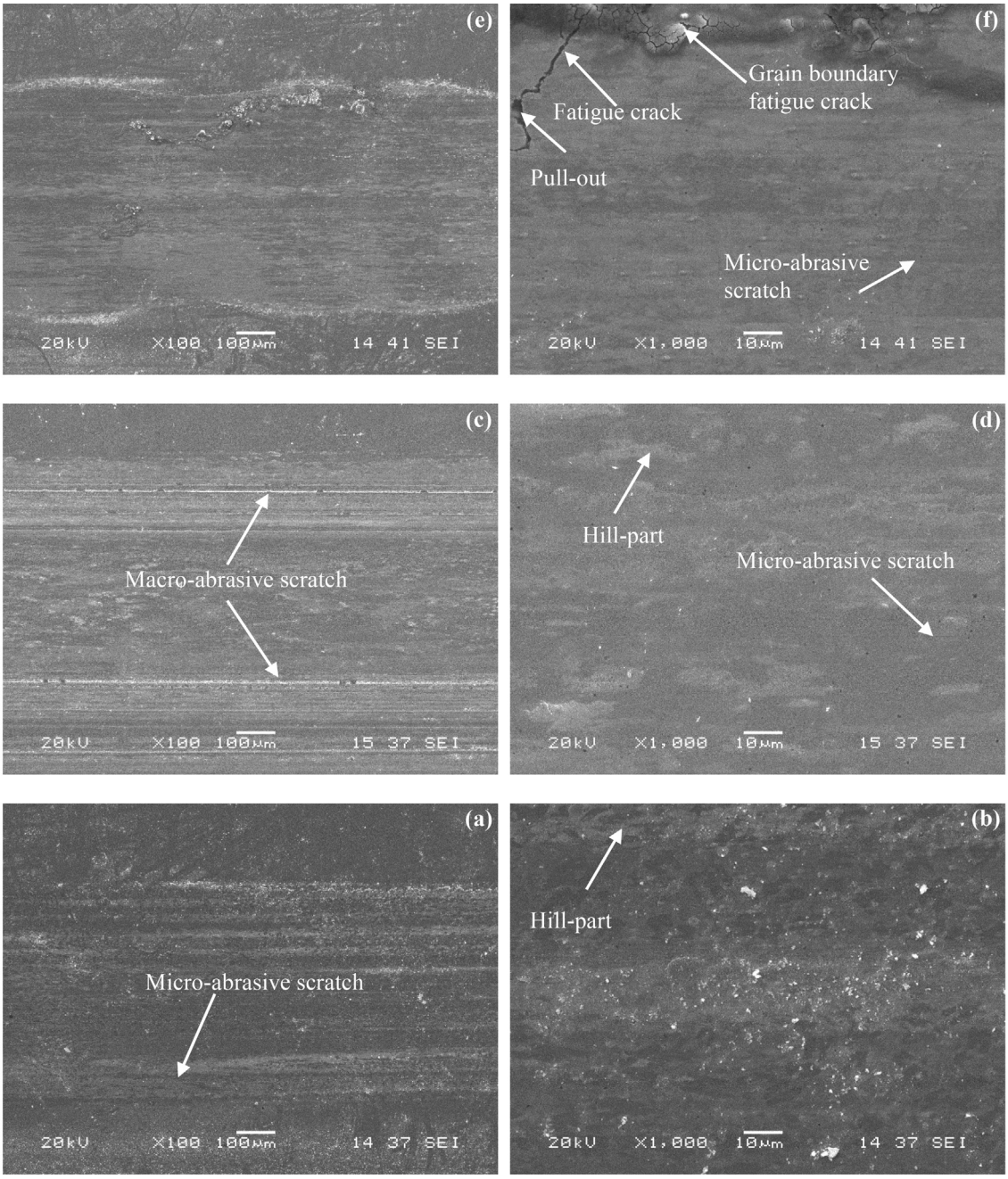

Fig. 9. Wear trace of surface alloyed layers under 5 N a-b) $Fe_{11}Cr_5(B,C)_4$c-d) $Fe_{13}Cr_4(B,C)_4$ and e-f) $Fe_{12}Cr_3(B,C)_4$ alloys.

so elastic modulus and hardness of these phases are much higher than that of the matrix [26,27]. In the metal matrix composite structures, increase in reinforced hard phases in the matrix caused to increase of the composite hardness and wear resistance according to well-known Archard's rules [28,29]. As known, a decrease in dimensions of dispersed reinforced hard phases for the same volumetric scales caused to increase of the hardness and so wear resistance [30]. Here, dislocations movements restrict with dispersed hard phases and thus increase to the hardness of the composite structure. Eutectics of the steel matrix and carbo-boride phases caused to toughened and hardened structure formation, so hard phase in aggressive conditions can be broken with applied high load values. However, eutectic microstructure supports the hard carbo-boride phase with tough steel matrix with pearlite like structures. Primer carbo-boride phases of the chromium together with iron and eutectic grains of the pearlite-like microstructure caused to withstand of the in-situ composite structure in aggressive wear conditions.

In the present study, wear rates of the $Fe_{11}Cr_5(B,C)_4$, $Fe_{12}Cr_4(B,C)_4$ and $Fe_{13}Cr_3(B,C)_4$ surface alloyed steels ranged from 3.07×10^{-5} mm^3/m to 4.23×10^{-5} mm^3/m, 3.89×10^{-5} mm^3/m to 5.8×10^{-5} mm^3/m and 4.2×10^{-5} mm^3/m to 6.95×10^{-5} mm^3/m, respectively.

The study agrees with G. Hu et al. study that increases in the load value caused an increase in wear rates [31]. G. Cui et al.'s study showed that the Fe-Cr-B surface alloyed layers showed on the order of ~10^{-4} mm^3/m wear rates [25]. Whereas, in the present study, wear rates ten times lower than that of the G. Cui et al. study. The carbon may exist in the alloy composition caused an increase in wear resistance of the alloyed layer. A 150% increase

in load value (from 2 N to 5 N) leads to an increase of 22.2% wear rate for $Fe_{11}Cr_5(B,C)_4$ alloy; When the increase in load value is a 300% (from 2 N to 8 N), the increase in wear rate is 37.7%. This value for $Fe_{12}Cr_4(B,C)_4$ and $Fe_{13}Cr_3(B,C)_4$ alloys respectively; 19–49.1% and 23.8–65.5%, respectively. Wear rates of all alloys are generally close to each other. As can be seen from the graph, the increase in chromium content (for 8 N load) caused a decreased wear rate of 65.54%.

In Fig. 8, the result of EDS analysis taken from the surface after wearing under 5 N load of the coated with $Fe_{12}Cr_4(B,C)_4$ composition is given. The SEM picture shows that wear products accumulate along the wear track. In EDS analysis, it is seen that there is oxygen in addition to elements such as carbon, boron, chromium and iron in its composition. Therefore, oxidative, micro-abrasive with the polishing process has developed as a general wear mechanism in all samples. However, in the SEM pictures taken after the wear test with 5 N load given in Fig. 9, it is understood that different wear mechanisms have developed in the samples. It is seen in Fig. 9b that the hard phases formed along the grain boundary cause fatigue cracks. These phases in the eutectic composition ((α-(Fe-Cr) +$(Fe,Cr)_{23}(C,B)_6$)) withstand damage during wear, but the matrix was pitted under the adhesive wear effect. Therefore, fatigue wear mechanism is also observed in this composition. A similar mechanism is observed in the study conducted by Torabinejad et al. [32]. In Fig. 9d, it is seen that the hill parts, which are hard phases, are not affected by abrasion, but, soft phases are worn. In addition, micro-abrasive lines can be clearly distinguished on the worn surface. Therefore, adhesive abrasive and polishing type wear mechanisms have developed during the wear of this composition. Similarly, it is seen that the coating with $Fe_{11}Cr_5(B,C)_4$ composition given in Fig. 9f does not have any cracks in the SEM picture and block phases are resistant to abrasion, but the matrix phase is pitting. This shows that the coating contains polishing type wear. It is known that the chromium added to the steel increases its toughness. In addition, the increasing chromium ratio contributes to both the hardness of the matrix and hardness with blocky hard carbo-boride phases. In the wear tests carried out in the study, it is observed that the fatigue wear mechanism develops in the coating with the decrease of the chromium ratio. Therefore, increasing chromium ratio contributes to the wear resistance of the coating.

3.3. Corrosion behavior

Fig. 10 shows the Tafel plots derived from the potentiodynamic polarization curves of alloyed surface layers. The curves indicate

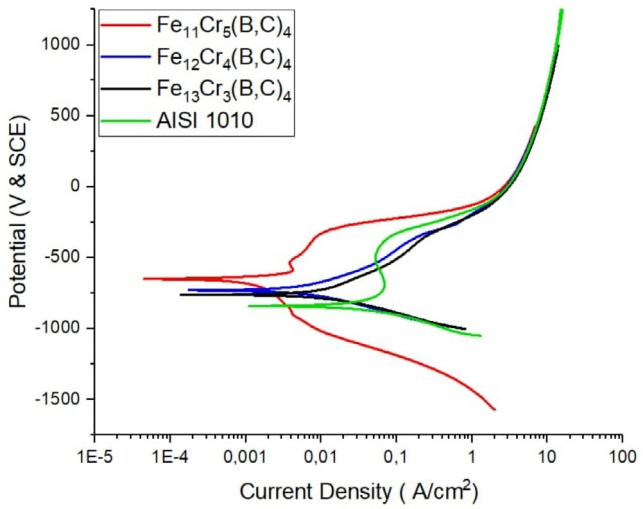

Fig. 10. Potentiodynamic polarization curves of coating layers.

that Cr content has a considerable effect on the corrosion behavior of the surface alloyed layers. It is observed from the curves that the current decreases with the increase of the potential of the cathodic region. This behavior states that corrosion occurs with an activation-controlled mechanism. It has been reported that negative potentials in Tafel curves increase the cathodic reaction rate required for metal dissolution. It is seen that the corrosion potential increases with the increase of the amount of chromium in the electrode cover composition. Corrosion potential of the coating made with an electrode with 15 %at. chromium content increased by 10% compared to the substrate material. It is seen that the increase is approximately 16% in the surface coated with the electrode with 25% (at.). chromium content.

Table 4 shows the data obtained from the potentiodynamic polarization curves. While the corrosion potential increases with the increasing amount of chromium, the current density decreases. According to Galvele, current density values are directly related to the electrode potentials and can give more accurate results about the electrochemical behavior of the material [33]. It is known that there will be an increase in corrosion resistance with decreasing current density. According to these results, it can be said that the coating has turned into a nobler character with increasing chromium ratio.

The coatings contain a-matrix (Fe-Cr) as well as other carboboride phases depending on the chromium ratio of the structure, as stated in microstructural studies. The main electrochemical reaction expected to be in the A-matrix structure is an oxidation reaction, and the corrosion reactions of iron-based alloys in a containing dissolved oxygen near-neutral pH may be generally written as following [34,35];

$$\text{Anodic reaction}: Fe \rightarrow Fe^{+2} + 2e^{-} \quad (6)$$

$$\textit{Cathodic reaction}: 1/2O_2 + H_2O + 2e^{-} \rightarrow 2OH^{-} \quad (7)$$

Cathodic reaction can be with oxygen reduction.
Overall reaction;

$$2Fe + 2H_2O + O_2 \rightarrow 2Fe^{+2} + 4OH^{-} \rightarrow 2Fe(OH)_2 \quad (8)$$

On the other hand, another factor that determines the chemical stability of a-matrix is chromium dispersed in the structure.

$$\textit{Anodic reaction}: Cr \rightarrow Cr^{+++3} + 3^{-} \quad (9)$$

As known, chromium content in the steels caused the formation of Cr_2O_3 adhesive layer on the surface and, the increase in the Cr content caused the increase of corrosion resistance because of the formation of more Cr_2O_3 layer. General Cr_2O_3 reaction in 3.5% NaCl aqueous solution for the Fe–Cr alloys is shown following [36];

$$4NaCl + Cr_2O_3 + 2H_2O + 3/2O_2 \rightarrow Na_2CrO_4 + HCl \quad (10)$$

Also, the contribution of other phases in the structure to the corrosion resistance affects the total corrosion resistance of the coating. As the chromium ratio increases, the amount of free chromium in the matrix phase will increase. This case will contribute to the corrosion resistance of the coating. However, corrosion potential of carbide and boride phases may be nobler than that of the matrix due to their low free energy. For instance, the corrosion potential of (α-(Fe-Cr)+$(Fe,Cr)_{23}(C,B)_6$) is believed to be nobler than that of α-(Fe-Cr) matrix. The chromium content of $(Fe,Cr)_{23}(C,B)_6$ is higher than that of the eutectic matrix (α-(Fe-Cr)+ $(Fe,Cr)_{23}(C,B)_6$). Also, the minor phases such as $(Fe,Cr)_2(C,B)$ and $(Fe,Cr)_7C_3$ contribute to the corrosion resistance of the surface coating. As a result, the coating containing mainly $M_{23}(C,B)_6$ and minor $M_7(C,B)_3$ phases may change the corrosion potential [9,37–39].

In Fig. 11, the SEM image of the corroded surfaces after polarization test is given. Some residues have appeared on the surfaces of

Table 4
Potentiodynamic polarization test results of corroded layers

Electrode	Ecorr mV	Icorr μA/cm^2	βa V/decade	Bc V/decade	Corrosion Rate mpy
$Fe_{11}Cr_5(B,C)_4$	−704.786	1.813	490	473.2	1.197
$Fe_{12}Cr_4(B,C)_4$	−727.256	6.069	196	146	4.309
$Fe_{13}Cr_3(B,C)_4$	−745.792	9.965	218.3	144.3	6.088
AISI 1010	−849.68	50.341	1227.1	159	30.757

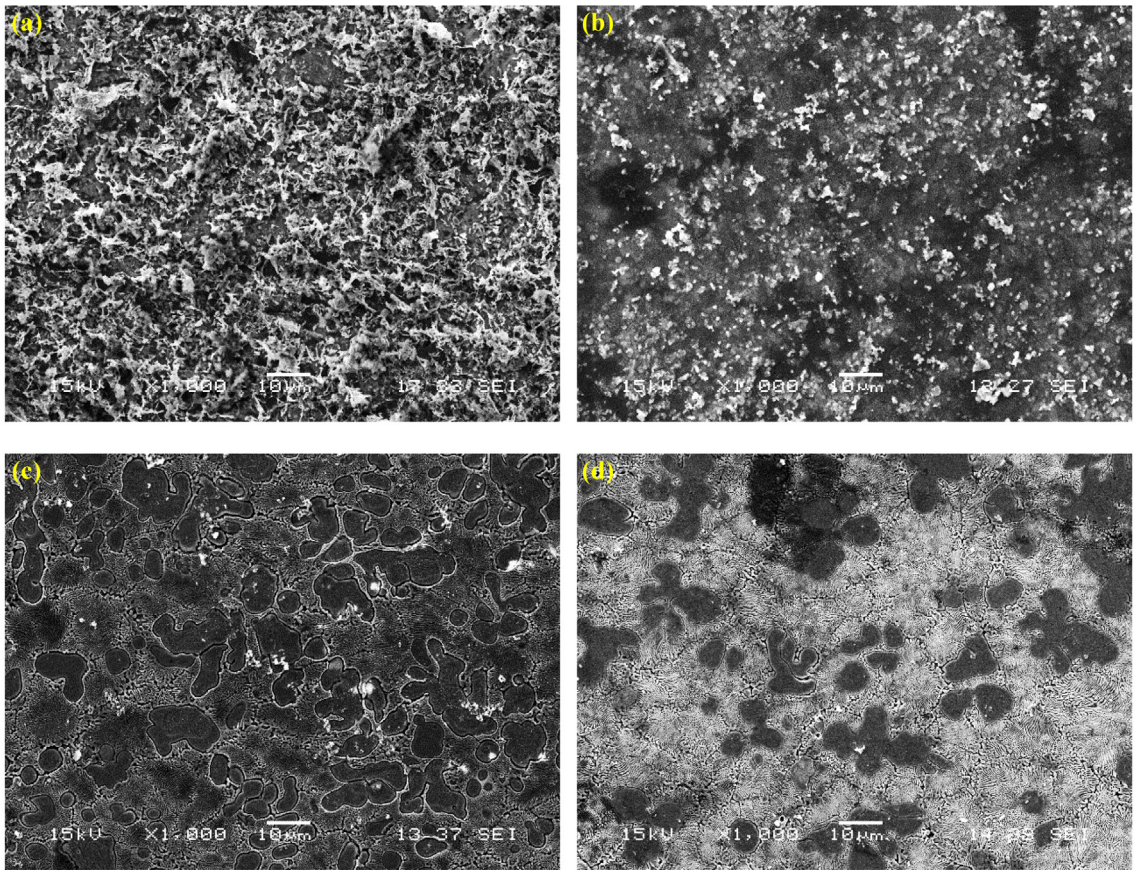

Fig. 11. Corroded surfaces of hardfaced with various Cr contents a)Substrate (AISI 1010) b)$Fe_{11}Cr_5(B,C)_4$c)$Fe_{12}Cr_4(B,C)_4$ d)$Fe_{13}Cr_3(B,C)_4$.

Fig. 11(a) and (b). This can be explained that the fluctuations in the anodic parts of the Tafel curves occur due to the separation of the protective layer from the surface [40]. It may indicate that the fluctuations in the Tafel curve of the substrate given in Fig. 9 and the $Fe_{11}Cr_5(B,C)_4$ coating layer are associated with this surface layer that forms on the surface and then breaks and accumulates.

There are partial gaps between the matrix phase and the structured eutectic phases in Fig. 11(c) and (d). Grabke et al. indicated that molecular chlorine penetrating the grain boundaries could react with $M_{23}C_6$ type carbides. Chlorine can react with $M_{23}C_6$ type carbide in the presence of oxygen via grain boundaries according to the reaction below. The chlorine required for the reaction is obtained by reacting HCl in Reaction (6) with dissolved oxygen in solution. Such a situation harms the corrosion resistance of the coating [36,41].

$$Cr_{23}C_6 + 23Cl_2 + 3O_2 \rightarrow 23CrCl_2 + 6CO \quad (11)$$

Another matter that affects the corrosion resistance is the silicon that can come from ferroalloys. Silicium is not present in carbide or boride phases and is dissolved in the matrix phase [42]. Generally, silicon dissolved in the matrix is thought to contribute to the corrosion resistance of the coating [9]. Consequently, it is seen that the corrosion rate decreases with increasing chromium content. This is an expected result due to the high corrosion resistance of the phases formed by chromium and the chromium being galvanically nobler than iron. Therefore the $Fe_{11}Cr_5(B,C)_4$ coating exhibit superior corrosion resistance as compared to the others.

4. Conclusions

In the present work, three different chemical compositions of $Fe_{(16-X)}Cr_X(B,C)_4$ (X = 3,4,5) surface alloying electrodes were produced successfully. SMAW techniques were used for surface alloying treatment. The following results have been obtained.

1. All the compositions of the surface alloyed layers include similar phases. However, SEM, EDX and elemental mapping studies shows that the $Fe_{11}Cr_5(B,C)_4$ alloy composition presents the hypereutectic microstructure which has blocky hard carboboride major phase ($M_{23}(C,B)_6$) together with eutectic (α-(Fe-Cr) + $M_{23}(C,B)_6$) besides $(Fe,Cr)_2(C,B)$ and $(Cr,Fe)_7(C,B)_3$ minor phases. However, the pre-eutectic microstructure is exhibited in $Fe_{13}Cr_3(B,C)_4$ and $Fe_{12}Cr_4(B,C)_4$ compositions. α-(Fe,Cr) + eutectic (α-(Fe-Cr) + $M_{23(}C,B)_6$) microstructure formed. However,

the decrease in the chromium and carbon content caused increase in the α-(Fe-Cr) content and the decrease in the eutectic (α-(Fe-Cr) + M_{23} $(C,B)_6$) content in the microstructure.

2. Dry sliding wear tests results showed that the coefficient of friction changes between 0.55 and 0.79 depending on the alloy compositions and wear test parameters. The coefficient of friction decreased with increase in applied load for all compositions. In the wear test, increase in load value leads to increase of wear rate for all compositions.
3. The Corrosion test showed that an increase in Cr content of the surface alloyed layer caused decrease in corrosion current. In the present study, $Fe_{11}Cr_5(B,C)_4$ has the highest Cr content and it has the highest corrosion resistance than that of the $Fe_{12}Cr_4(B,C)_4$ and $Fe_{13}Cr_3(B,C)_4$. Corrosion rate decreases with increasing chromium content. It is clearly evident from the corrosion results that the $Fe_{11}Cr_5(B,C)_4$ coating exhibits superior corrosion resistance compared to the other surface alloying and substrate materials.

Declaration of Competing Interest

The authors declare that they have no known competing financial interests or personal relationships that could have appeared to influence the work reported in this paper.

Acknowledgement

Authors are grateful to the financial support provided by TUBITAK (Turkey Scientific and Technological Research) with Project No. 219M192.

References

[1] R. Zahiri, R. Sundaramoorthy, P. Lysz, C. Subramanian, Hardfacing using ferro-alloy powder mixtures by submerged arc welding, Surface Coat. Technol. 260 (2014) 220–229.
[2] D.-B. Wei, H.-X. Liang, S.-Q. Li, F.-K. Li, F. Ding, S.-Y. Wang, Z.-L. Liu, P.-Z. Zhang, Microstructure and tribological behavior of W-Mo alloy coating on powder metallurgy gears based on double glow plasma surface alloying technology, J. Min. Metall. B Metall. 55 (2) (2019) 227–234.
[3] X. Wang, F. Han, X. Liu, S. Qu, Z. Zou, Microstructure and wear properties of the Fe – Ti – V – Mo – C hardfacing alloy, 265 (2008) 583–589, 10.1016/j.wear.2007.12.001.
[4] H.Z. Oo, P. Muangjunburee, Wear behaviour of hardfacing on 3.5% chromium cast steel by submerged arc welding, Mater. Today:. Proc. 5 (3) (2018) 9281–9289.
[5] J.-H. Chen, C.-C. Hsieh, P.-S. Hua, C.-M. Chang, C.-M. Lin, P.-T.-Y. Wu, W. Wu, Microstructure and abrasive wear properties of Fe-Cr-C hardfacing alloy cladding manufactured by Gas Tungsten Arc Welding (GTAW), Met. Mater. Int. 19 (1) (2013) 93–98, https://doi.org/10.1007/s12540-013-1015-4.
[6] S. Babu, V. Balasubramanian, G. Madhusudhan Reddy, T.S. Balasubramanian, Improving the ballistic immunity of armour steel weldments by plasma transferred arc (PTA) hardfacing, Mater. Design (1980-2015) 31 (5) (2010) 2664–2669.
[7] M. Bahoosh, H.R. Shahverdi, A. Farnia, Macro-indentation fracture mechanisms in a super-hard hardfacing Fe-based electrode, Eng. Fail. Anal. 92 (2018) 480–494.
[8] Y.A. Joo, T.S. Yoon, S.H. Park, K.A. Lee, Microstructure and compression properties of Fe-Cr-B alloy manufactured using laser metal deposition, Arch. Metall. Mater. 63 (3) (2018) 1459–1462, https://doi.org/10.24425/123828.
[9] G. Azimi, M. Shamanian, Effects of silicon content on the microstructure and corrosion behavior of Fe–Cr–C hardfacing alloys, J. Alloy. Compd. 505 (2) (2010) 598–603.
[10] L. Lu, H. Soda, A. McLean, Microstructure and mechanical properties of Fe–Cr–C eutectic composites, Mater. Sci. Eng., A 347 (1-2) (2003) 214–222.
[11] H. Berns, A. Fischer, Microstructure of Fe-Cr-C hardfacing alloys with additions of Nb, Ti and, B, Mater. Charact. 39 (2-5) (1997) 499–527.
[12] C. Fan, M.-C. Chen, C.-M. Chang, W. Wu, Microstructure change caused by (Cr, Fe)23C6 carbides in high chromium Fe–Cr–C hardfacing alloys, Surf. Coat. Technol. 201 (3-4) (2006) 908–912.
[13] A. Inoue, T. Masumoto, Carbide reactions (M3C{\textrightarrow}M7C3 {\textrightarrow}M23C6{\textrightarrow}M6C) during tempering of rapidly solidified high carbon Cr-W and Cr-Mo steels, Metall. Trans. A 11 (5) (1980) 739–747, https://doi.org/10.1007/BF02661203.
[14] K. Yamada, H. Ohtani, M. Hasebe, Thermodynamic analysis of the Fe-Cr-B ternary system, High Temp. Mater. Process. 27 (4) (2008) 269–284, https://doi.org/10.1515/HTMP.2008.27.4.269.
[15] B. Predel, B-Cr (Boron-Chromium), in: O. Madelung (Ed.), B-Ba – C-Zr, Springer, Berlin Heidelberg, Berlin, Heidelberg, 1992, pp. 1–3.
[16] J.C.J. Gigolotti, V.M. Chad, M.I.S.T. Faria, G.C. Coelho, C.A. Nunes, P.A. Suzuki, Microstructural characterization of as-cast Cr–B alloys, Mater. Charact. 59 (1) (2008) 47–52.
[17] Y.F. Zhou, Y.L. Yang, J. Yang, D. Li, Y.W. Jiang, X.J. Ren, Q.X. Yang, Effect of titanium content on microstructure and wear resistance of fe-cr-c hardfacing layers, Weldiing J. 91 (March) (2012) 229–235.
[18] S. Liu, Y. Zhou, X. Xing, J. Wang, Y. Yang, Q. Yang, Agglomeration model of (Fe, Cr)7C3 carbide in hypereutectic Fe-Cr-C alloy, Mater. Lett. 183 (2016) 272–276.
[19] J.-X. Gong, D. Li, Y.-F. Xiao, Q.-H. Zhang, Microstructure and wear resistance of Fe-Cr-B-C hardfacing alloys, Cailiao Rechuli Xuebao/Transactions Mater. Heat Treat. 31 (3) (2010) 136–141.
[20] M.V. Radchenko, V.G. Radchenko, A.M. Kirienko, Y.O. Shevtsov, Evaluating the hardness and ductility of coatings formed by electron-beam hard-facing in a vacuum, Metallurgist 41 (7-8) (1997) 264–267.
[21] R. Sahara, T. Matsunaga, H. Hongo, M. Tabuchi, Theoretical investigation of stabilizing mechanism by boron in body-centered cubic iron through (Fe, Cr)23(C, B)6 precipitates, Metall. Mater. Trans. A 47 (5) (2016) 2487–2497, https://doi.org/10.1007/s11661-016-3397-7.
[22] B. Venkatesh, K. Sriker, V.S.V. Prabhakar, Wear characteristics of hardfacing alloys: State-of-the-art, Procedia Mater. Sci. 10 (2015) 527–532.
[23] M.H. Amushahi, F. Ashrafizadeh, M. Shamanian, Characterization of boride-rich hardfacing on carbon steel by arc spray and GMAW processes, Surf. Coat. Technol. 204 (16-17) (2010) 2723–2728.
[24] C. Özel, T. Gürgenç, O. Yiğit, Comparison of microstructure and microhardness of Fe-Cr-W-B-C and Fe-Cr-B-C coating on low carbon steel coted with PTA method, in R. Halıcıoğlu, H. Akın Kırlı, Y. Fedai (Eds.), Int. Adv. Res. Eng. Congr. 2017, Osmaniye, (2017): pp. 743–751.
[25] C. Gongjun, J. Wei, W. Gongxiong, Wear behavior of Fe-Cr-B alloys under dry sliding condition, Ind. Lubr. Tribol. 67 (4) (2015) 336–343, https://doi.org/10.1108/ILT-07-2014-0065.
[26] L.i. Guo-lu, L.i. Ya-long, D. Tian-shun, F.u. Bin-Guo, W. Hai-dou, Z. Xiao-dong, Z. Xiu-kai, Microstructure and interface characteristics of NiCrBSi thick coating remelted by TIG process, Vacuum 156 (2018) 440–448.
[27] V. Torabinejad, M. Aliofkhazraei, A.S. Rouhaghdam, M.H. Allahyarzadeh, Tribological properties of Ni-Fe-Co multilayer coatings fabricated by pulse electrodeposition, Tribol. Int. 106 (2017) 34–40.
[28] V.K. Rai, R. Srivastava, S.K. Nath, S. Ray, Wear in cast titanium carbide reinforced ferrous composites under dry sliding, Wear 231 (2) (1999) 265–271.
[29] V. Torabinejad, M. Aliofkhazraei, A. Sabour Rouhaghdam, M.H. Allahyarzadeh, Tribological Behavior of Electrodeposited Ni-Fe Multilayer Coating, Tribol. Trans. 60 (5) (2017) 923–931, 10.1080/10402004.2016.1230687.
[30] Z. Mahidashti, M. Aliofkhazraei, N. Lotfi, Review of nickel-based electrodeposited tribo-coatings, Trans. Indian Inst. Met. 71 (2) (2018) 257–295.
[31] G.e. Hu, H. Meng, J. Liu, Friction and sliding wear behavior of induction melted FeCrB metamorphic alloy coating, Appl. Surf. Sci. 308 (2014) 363–371.
[32] V. Torabinejad, M. Aliofkhazraei, A.S. Rouhaghdam, M.H. Allahyarzadeh, Tribological performance of Ni-Fe-Al2O3 multilayer coatings deposited by pulse electrodeposition, Wear 380-381 (2017) 115–125.
[33] J.R. Galvele, Tafel's law in pitting corrosion and crevice corrosion susceptibility, Corros. Sci. 47 (12) (2005) 3053–3067, https://doi.org/10.1016/j.corsci.2005.05.043.
[34] B. Lu, J. Luo, S. Chiovelli, Corrosion and wear resistance of chrome white irons – A correlation to their composition and microstructure, Metall. Mat. Trans. A 37 (10) (2006) 3029–3038.
[35] C.M. Chang, C.M. Lin, C.C. Hsieh, J.H. Chen, C.M. Fan, W. Wu, Effect of carbon content on microstructural characteristics of the hypereutectic Fe-Cr-C claddings, Mater. Chem. Phys. 117 (1) (2009) 257–261, https://doi.org/10.1016/j.matchemphys.2009.05.052.
[36] M. Paneru, G. Stein-Brzozowska, J. Maier, G. Scheffknecht, Corrosion mechanism of alloy 310 austenitic steel beneath NaCl deposit under varying SO2 concentrations in an oxy-fuel combustion atmosphere, Energy Fuels 27 (10) (2013) 5699–5705, https://doi.org/10.1021/ef4005626.
[37] C.-M. Chang, C.-C. Hsieh, C.-M. Lin, J.-H. Chen, C.-M. Fan, W. Wu, Effect of carbon content on microstructure and corrosion behavior of hypereutectic Fe–Cr–C claddings, Mater. Chem. Phys. 123 (1) (2010) 241–246.
[38] Y. Kayali, A. Büyüksağiş, Y. Yalçin, Corrosion and wear behaviors of boronized AISI 316L stainless steel, Met. Mater. Int. 19 (5) (2013) 1053–1061.
[39] M. Erdogan, I. Gunes, Corrosion Behavior and Microstructure of Borided Tool Steel, Matéria (Rio J.) 20 (2) (2015) 523–529.
[40] H. Eren, Ferritik Paslanmaz Çeliğin Korozyon Davranışına Karbür Yapıcı Elementlerin Etkilerinin İncelenmesi, Fırat Üniversitesi (2005).
[41] D.E. Von Legierungselementen, The influence of alloying elements on the chlorine-induced high temperature corrosion of Fe-Cr alloys in oxidizing atmospheres 578 (1999) 561–569.
[42] A. Sorour, Microstructure and Tribology of Fe–Cr–B-Based Alloys, McGill University (2014).